Active Skin for Turbulent Drag Reduction

Othon K. Rediniotis[a], Dimitris C. Lagoudas[a], Raghavendran Mani[a]
Aerospace Engineering Department, Texas A&M University,
College Station, TX 77843-3141
Tel: (979) 845-0708, Fax: (979) 845-6051

George Em Karniadakis[a]
Professor, Division of Applied Mathematics
Brown University, Providence, RI 02912
Tel: (401) 863-1217; Fax: (401) 863-3369

ABSTRACT

Drag reduction for aerial vehicles has a range of positive ramifications: reduced fuel consumption with the associated economic and environmental consequences, larger flight range and endurance and higher achievable flight speeds. This work capitalizes on recent advances in active turbulent drag reduction and active material based actuation to develop an active or "smart" skin for turbulent drag reduction in realistic flight conditions. The skin operation principle is based on computational evidence that spanwise traveling waves of the right amplitude, wavelength and frequency can result in significant turbulent drag reduction. Such traveling waves can be induced in the smart skin via active-material actuation. The flow control technique pursued is "micro" in the sense that only micro-scale wave amplitudes (order of 30μm) and energy inputs are sufficient to produce significant benefits. Two actuation principles have been proposed and analyzed. Different skin designs based on these two actuation principles have been discussed. The feasibility of these different actuation possibilities (such as Shape Memory Alloys and Piezoelectric material based actuators) and relative merits of different skin designs are discussed. The realization of a mechanically actuated prototype skin capable of generating a traveling wave, using a rapid prototyping machine, for the purpose of validating the proposed drag reduction technique is also presented.

Keywords: Shape Memory Alloys, Piezoelectric materials, Turbulent Drag, Actuator, Active Skin

1. INTRODUCTION

Turbulence control methods have been developed under the assumption that the turbulence production cycle could be favorably altered, stabilized, or reduced in intensity by the manipulation and alteration of low-speed streaks, quasi-streamwise vortices, the viscous sublayer, or the hairpin-like structures that populate the near-wall region. To this end, the use of small grooves or riblets mounted on the wall surface has proved to be effective in partially suppressing turbulence and reducing the drag force by about 5% to 10% [1,2]. However, to date none of the drag reduction techniques used in practice has been able to eliminate the near-wall streaks, which is the main source of turbulence production. In recent work, a new fundamental mechanism was revealed, which could completely eliminate the near-wall streaks[3]. It was based on the application of a force traveling wave along the *spanwise* direction acting within the viscous sublayer and with the force decaying exponentially away from the wall. In particular the following traveling wave force was used:

$$F_z = Ie^{-\frac{y}{\Delta}} \sin\left(\frac{2\pi}{\lambda} z - \frac{2\pi}{T} t\right) \tag{1}$$

[a] Further Author information: (Send correspondence to O.K.R)
O.K.R.: e-mail: rediniotis@aero.tamu.edu
D.C.L.: e-mail: dlagoudas@aero.tamu.edu
R. Mani: e-mail: raghav@tamu.edu
G.E.K.: e-mail: gk@cfm.brown.edu

where I is the amplitude of excitation, λ is the wavelength (along the span), T is the time period and Δ is the penetration depth. The main effect of the action of the traveling wave, when it is effective in reducing the drag force on the controlled wall, is to weaken and in many cases to completely eliminate the wall streaks. The numerical simulations showed that the action of the traveling wave of certain characteristics could result in drag reduction on the order of 50%.

It was observed that the phase speed of the traveling wave needed to be at least one-third of the free stream velocity. This condition in turn enforces either a lower bound on frequency or a lower bound on the wavelength of the traveling wave. Furthermore, maximum drag reduction was achieved when the penetration depth, Δ, is of the order of the dimensions of the viscous sublayer. This relatively small requirement for the penetration of the exciting force into the fluid is an encouraging factor to investigate surface based actuation techniques as cost-effective actuation candidates.

The force wave utilized in the numerical simulations can be realized by the use of a skin that would deform to generate a surface-deformation traveling wave. The skin could be attached to the surface of an aircraft wing, for example, and be deformed to the shape of the required wave using actuators made of active materials. A traveling wave motion can then be achieved by changing the points of actuation in a serial fashion. Parametric studies indicate that for typical Reynolds numbers encountered during flight conditions in Unmanned Aerial Vehicles (UAVs), the parameters of the surface wave were: Wavelength (λ) ~ 25mm, Frequency (ν) ~ 50 Hz & Amplitude = 30 μm (which corresponds to the penetration depth). The amount of actuation required would be therefore very small since micro-scale wave amplitudes (order of 30μm) are sufficient to produce significant turbulent drag reduction. However, for higher Reynolds numbers, encountered for example in aircraft flight, smaller wavelengths and higher frequencies (order of several hundred Hz) are required.

2. PRINCIPLES OF ACTIVE TRAVELING WAVE SKIN

In this work two possible actuation principles for the active skin that can achieve a surface traveling wave are discussed. The first actuation principle is depicted as a free body diagram in Figure 1. Consider a long plate subjected to equally spaced external moments that are equal in value but alternate in sign. This loading pattern can generate a static wave profile, from which a traveling wave can be realized by shifting the points of application of the moments. The moment can be realized either by the application of equal and opposite forces (couple) at those points or by unbalanced lateral forces separated by a lever arm.

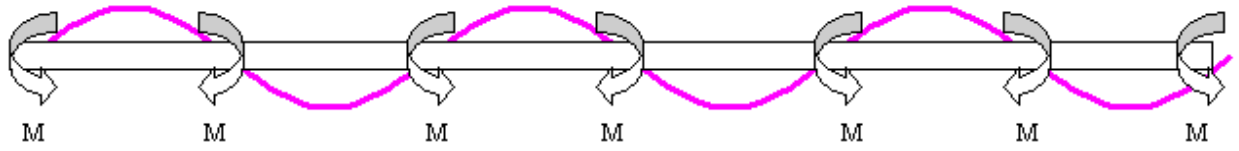

Figure 1. Moment based Actuation Principle.

The second actuation principle utilizes equally spaced vertical external forces along the length of the skin. The amplitudes and the directions of these forces vary periodically in order to match the skin deflection required as shown in Figure 2.

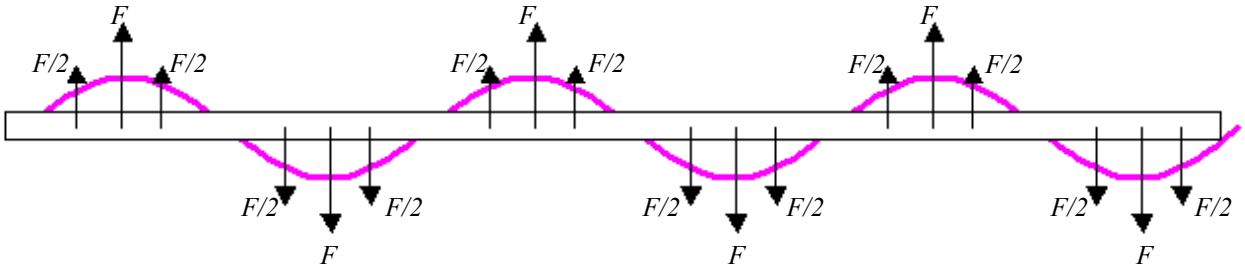

Figure 2. Force based Actuation Principle.

This second actuation principle can also be viewed as a more general form of the first actuation principle with the values of the actuating moments varying in a periodic manner instead of being constant. A traveling wave profile can be generated by simultaneously varying all the forces in a periodic manner. All the forces would oscillate with the same frequency and the same amplitude. However each successive force would lag the previous force by a constant phase difference. Since the deflections would be in phase with the forces, the net effect would be a traveling wave.

3. THEORETICAL ANALYSIS

3.1. Periodicity Assumption

To simplify the analysis, it is possible to utilize the inherent periodicity in loading and boundary conditions of the active skin, to reduce the analysis domain to a "Unit Cell". The Unit Cell can be defined as the smallest repeating unit of the active skin, the behavior of which would completely describe the behavior of the entire skin. The analytical expressions for the deflection amplitude and the natural frequency of the Unit Cell can be obtained by solving the general expressions that describe cylindrical bending in plates. Utilizing the periodicity assumption the Unit Cells for the two actuating principles shown in Figure 1 and Figure **2** can be obtained as the section of skin that is one wavelength long. Utilizing the symmetry in the bending, the Unit Cell can be further reduced to a section of the skin that is half a wavelength long (Figure 3).

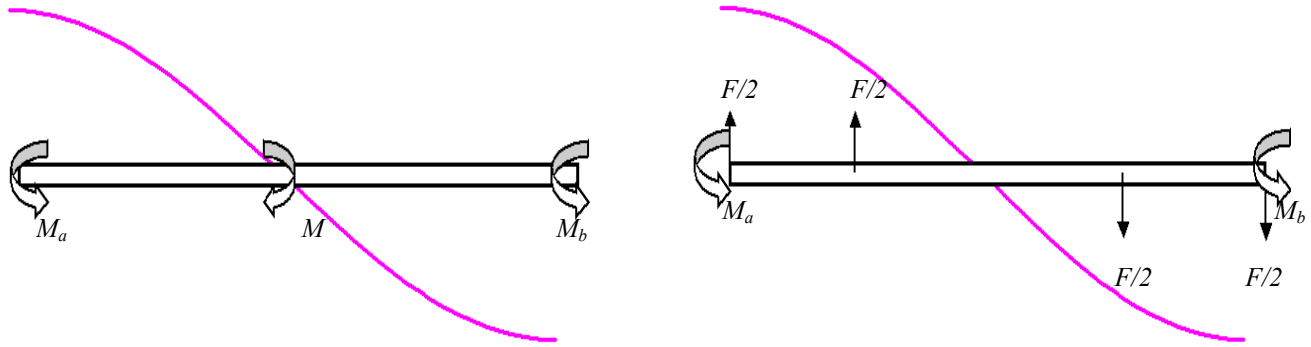

Figure 3. Unit Cells for the two actuation principles.

The appropriate boundary conditions for the Unit Cell would therefore be

- *Symmetry conditions at the ends*
- *Zero deflection for the point in the middle of the Unit Cell*

(M_a and *M_b* are the boundary conditions for the Unit Cell that need to be solved for and are not the externally applied moments. In the free body diagram of the Unit Cell for the force based actuation technique, the forces at the ends are half the values of the actual forces at these points since the effect of these forces are equally shared by two adjoining Unit Cells.)

3.2 Analytical Derivations

The governing equation for cylindrical bending in thin rectangular plates (linear elastic and isotropic material) undergoing small strains (in the absence of an elastic foundation) is given by the following equation [25-26]:

$$\frac{\partial^4 w}{\partial x^4} = \frac{1}{D}\left[q - \rho h \frac{\partial^2 w}{\partial t^2} + \frac{\rho h^3}{12} \frac{\partial^4 w}{\partial x^2 \partial t^2} + \frac{\partial^2 M_{xx}}{\partial x^2} \right] \tag{2}$$

where $D = Eh^3/12(1- \nu^2)$, w = deflection of the plate, E = Young's Modulus, ν = Poisson Ratio, h = thickness of the plate, q = applied vertical force/unit area, M_{xx} = Bending moment per unit length of the plate. In the absence of vertical loading and for a quasi-static case, the expression can be simplified to:

$$\frac{\partial^4 w}{\partial x^4} = \frac{1}{D}\frac{\partial^2 M_{xx}}{\partial x^2} \tag{3}$$

The Moment Area method developed for beam bending[27] can be extended to cylindrical bending of plates to solve for the deflection amplitudes. Solving for the moment and the shear force distribution in the Unit Cell and using the moment area method, the quasistatic deflection amplitudes for the two actuation principles are obtained as:

$$\Delta_1 = \frac{3F_1 bl^2(1-\nu^2)}{4Eh^3 d} \tag{4}$$

$$\Delta_2 = \frac{27F_2 l^3(1-\nu^2)}{64Eh^3 d} \tag{5}$$

where: Δ_1 and Δ_2 are the deflection amplitudes for the first and second principles of actuation respectively; l is length of the Unit Cell; d is the width of the Unit Cell; F_1 and b are the load and the load arm through which the external moment is generated.(i.e. $M = F_1 b$) for the moment based actuation and F_2 is the force amplitude for the force based actuation.

For the case of free vibrations, ignoring the contribution from the rotational inertia term, the simplified differential equation is[28]:

$$\frac{\partial^4 w}{\partial x^4} = -\frac{\rho}{D}\frac{\partial^2 w}{\partial t^2} \tag{6}$$

The boundary conditions for this Eigenvalue problem are that the slopes at the edges of the Unit Cell are zero and that the point of application of the external moment is both a point of inflection and a point of zero displacement. Solving for these boundary conditions the expression for the n^{th} natural frequency (for both actuation principles) is obtained as:

$$f_n = \frac{\pi n^2 h}{2l^2}\sqrt{\frac{E}{12\rho(1-\nu^2)}} \tag{7}$$

where f_n = Natural Frequency and n = Eigenmode

3.3 Comparison of Work Efficiencies

The work done to generate the same deflection amplitudes, in the two actuation principles can be used to compare the efficiencies of the two principles. Assuming actuation under quasistatic conditions, the work done can be evaluated as the integral of the strain energy stored in the entire volume of the plate and is given in the case of moment based actuation principle by the expression:

$$W_1 = \frac{3b^2 l(1-\nu^2)}{2Eh^3 d}F_1^2 \tag{8}$$

Alternatively this expression can be obtained as half the product of the external moment and the angle of rotation at the point of application of the moment. The work done for the force based actuation principle is:

$$W_2 = \frac{23l^3(1-\nu^2)}{64Eh^3 d}F_2^2 \tag{9}$$

In a similar manner this same expression can be obtained by considering the sum of the individual contributions from each of the external forces (the points of application of the forces deflect in the direction of the forces). To generate the same deflections, the ratio of the forces needed for the two actuation principles is given by:

$$\frac{F_1}{F_2} = \frac{9}{16}\frac{l}{b} \tag{10}$$

Using this relationship the ratio of the work efficiencies is evaluated as:

$$\frac{W_1}{W_2} = 1.32 \tag{11}$$

Note that the ratio of the work inputs is independent of the dimensions of the plate. Therefore it can be concluded that from a structural point of view, the force based actuation principle is more efficient than the moment based actuation principle. However when it comes to actual implementation of these two concepts, there are many other factors that finally would determine which design is better suited for the application at hand and these would be discussed later.

3.4 Significance of Parametric Studies

The significance of identifying the relationship between the deflection amplitude/natural frequency and the skin dimensions lies in the fact that they greatly aid in estimating approximate model dimensions (L & h) based on performance requirements without actually attempting multiple iterations of finite element analysis. For example, it is obvious from the proportionalities that decreasing *Thickness (h)* is more effective in increasing Amplitude (or conversely in reducing force required for the same amplitude) than increasing *Length (L)*.

Consider a sample case that uses the moment actuation principle: L = 25mm, h=0.5mm with the material being Aluminum of E=70Gpa, ν=0.345 & ρ=2600 kgr/m^3; force applied is F_1=1N; load arm = b = 3mm long. For these parameters, the amplitude would be 41.29μm and the natural frequency would be equal to 8021.6 Hz.

Reducing the thickness by half, i.e. h = 0.25mm, results in a deflection amplitude of 330.34μm which is an order of magnitude greater than the response with h = 0.5mm. Conversely a force of just F = 0.1388N is sufficient in obtaining the earlier response of 41.29μm in this case. It is this kind of insight into the system that the parametric study provides that is very useful.

The value of natural frequency of the skin can also prove to be crucial. If the actuation frequency were to be made equal to the first natural frequency of the Unitcell, this would set the skin into resonance. Since the eigenmode shape corresponding to the first natural frequency is identical to the deflection pattern desired, this resonance phenomenon would greatly amplify the deflection pattern. Consequently it is expected that this resonance would bring down the force requirements and hence the actuation costs.

It can be mentioned generally that a reduction in thickness or an increase in length is beneficial in two ways. It not only results in an increase in the deflection amplitude for the same force but also in the reduction in the value of the first natural frequency. The latter effect is significant to our efforts in utilizing resonance to reduce actuation costs. By reducing the frequency from around 8kHz (h=0.5mm) to a value around 4kHz(h=0.25mm), it makes it possible to find realistic actuation strategies that can deliver forces at resonance frequencies. However there is an upper limit on the value of the wavelength (because of the requirement on the phase speed of the traveling wave), beyond which the efficiency of drag reduction would start dropping.

4. SKIN DESIGNS AND ACTUATION STRATEGIES

4.1 SMA actuator based Active Skin

Three different active skin designs that would be capable of creating a traveling wave form profile using either of the actuation principles have been considered. Figure 4 presents a cross section and a top view of the first skin design in its non-actuated state. This design works on the principle of moment based actuation. The moments that bend the skin are created by lateral forces that act on the skin through “legs” that are attached to the top surface of the skin. The legs can slide (left and right) with respect to the bottom surface (which is the surface attached to the vehicle) while the upper surface is exposed to the flow. The “legs” are actuated in a manner that induces rotation of the legs, which in turn results in a deformation of the top surface. When the legs are actuated in a coordinated manner it results in a wavy deformation pattern on the upper surface. This coordinated leg actuation/rotation can be achieved as described below.

A Shape Memory Alloy[4-20] (SMA) wire runs through the “legs”, through small holes on their sidewalls. The direction of the SMA wire is in the spanwise direction, while the major dimension of the “legs” is along the streamwise direction. Within each “leg” a circular flat disk is attached to the SMA wire, with its diameter significantly larger than the diameter of the holes on the sidewalls of the “legs”. Each SMA-disk joint is electrically connected to the electrical control circuit, and is powered independently. When a voltage difference is applied between the leftmost (“joint 1”) and the rightmost SMA-disk (“joint 5”) joints in Figure 4, the negative strain induced in the SMA (on account of the wire contracting) will cause the disks of joints 1 and 5 to contact the walls of legs 1 and 5 thus transferring to them the load generated by the SMA.

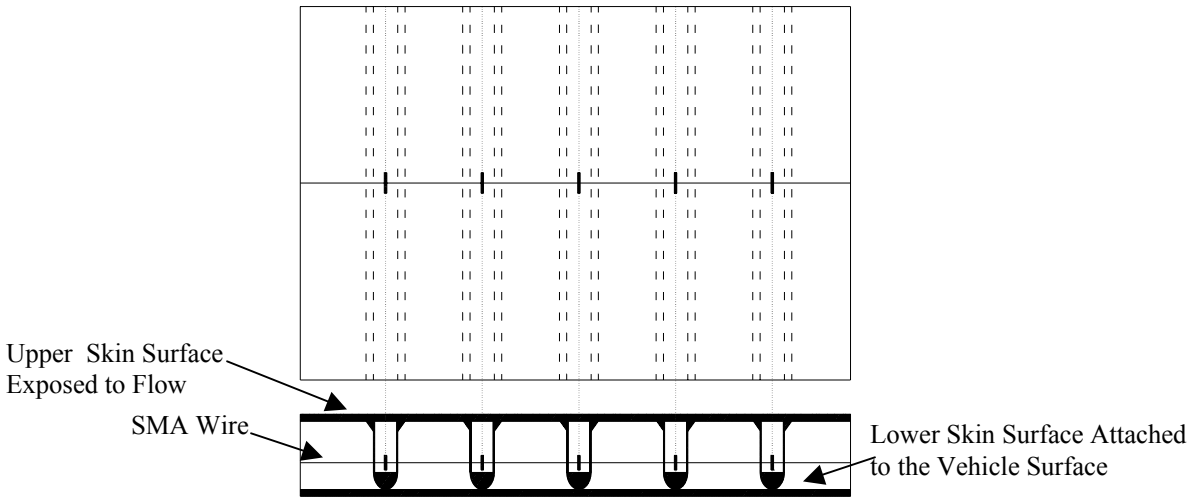

Figure 4. Cross section and top view of SMA actuated active skin.

Figure 5. Resulting waveform after actuating SMA sections between legs 1 and 5 and between legs 9 and 13 (y-dimensions have been magnified to illustrate the principle).

As shown in Figure 5 in an exaggerated fashion, as the SMA sections between legs 1 and 5 and between legs 9 and 13 contract, the SMA section between legs 5 and 9 will have to elongate/strain accordingly. Therefore the SMA sections between 1 and 5 and 9 and 13 will have to produce enough force not only to deform the upper skin but also to strain the SMA section between legs 5 and 9. This requirement is typical in antagonistic SMA actuators and presents no problem, since the sections between 1 and 5 and 9 and 13 are austenitic and have a much larger stiffness (2 to 3 times higher) than the section between 5 and 9, which is in the martensitic phase. One other point that deserves mention is that the bending caused by the actuation would not be exactly uniform all along the streamwise direction on account of the fact that the loading takes place at discrete points. But it is assumed that the deviation would be negligible if the SMA actuators were placed in relatively small intervals in the streamwise direction.

4.2 Piezoelectric C-Block actuator based Active Skin

SMAs are one of the possibilities discussed as possible mechanisms for actuation. The same structural design (i.e. the same actuation concept) can be actuated using Piezoceramic C-block actuators[21-23] for applications with very high Reynolds numbers, where the required actuation frequencies exceed the bandwidth SMAs are capable of. The individual C-block actuator, which is configured in a semi-circular shape, can be aligned in series or in parallel to optimize the force and deflection output to those required by the application at hand, while simultaneously fitting within the space constraints. Figure 6 illustrates the principles of piezoelectric actuation of the active skin in the second design. When electrical voltage is properly applied to a semi-circular, C-block piezoelectric actuator, positioned between two consecutive "legs" it causes the ends of the semi-circle to deflect radially inward, towards each other. This action causes displacement of the disks in the "legs" and subsequent "leg" deflection. The key to piezoelectric actuation will be to actuate locally in a time sequence that produces the desired traveling wave, without antagonizing with the neighboring structural elements and piezoelectric actuators. Direct attachment of piezoelectric patches on the skin, in the traditional way, will be avoided since it will result in interference from neighboring piezoelectric elements, thus increasing the actuation energy cost.

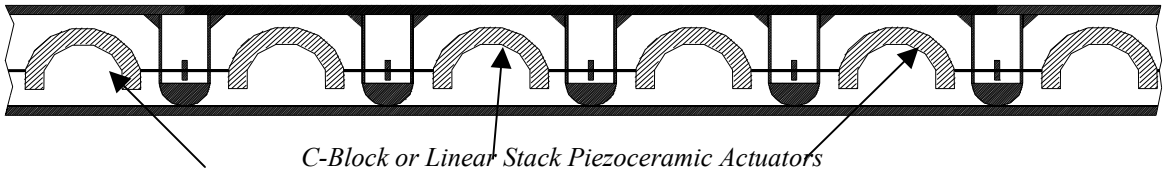

Figure 6. Piezoelectrically actuated active skin.

4.3 Piezoceramic Stack actuator based Active Skin

A third skin design is shown in Figure 7. This design works on the force based actuation principle. In this design the "legs" are replaced by linear Piezoceramic Stack Actuators[24] (PSAs), which actuate the skin in a direction along their axis. On actuation, the PSAs would exert a force on the skin in the vertical direction causing the skin to bend. By varying the values of the forces (in the PSAs) along the length of the skin in a periodic fashion it is possible to achieve a static bending in the form of sinusoidal wave. By varying the force applied by each PSA with time in a periodic fashion it would be possible to obtain a traveling wave. In effect the loading of the PSAs would be in phase with the displacement of the skin itself.

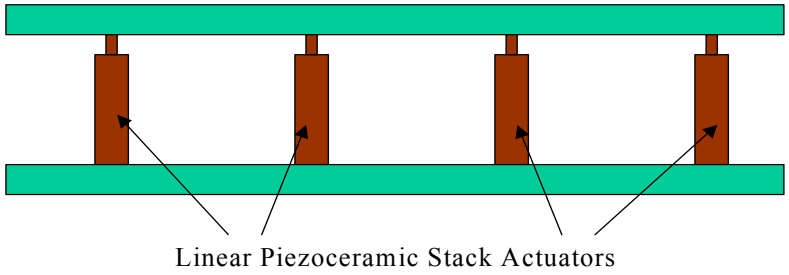

Figure 7. Skin design with linear piezoceramic stack actuators oriented perpendicular to the skin.

5. FINITE ELEMENT ANALYSIS

A parametric study using Finite Element Analysis was performed on the SMA based actuator design. A Plane Strain analysis of the Unit Cell was carried out using the Finite Element solver *ABAQUS*. Quadratic Plane Strain elements were used to mesh the model. The mesh was successively refined till further refinement did not produce any changes in the result up to the 5^{th} significant digit. The meshing corresponding to this accuracy has 4 quadratic plane strain elements in the thickness direction of the skin. The symmetry boundary condition implied that shear force and slope at the ends are zero. This was enforced by restricting the nodes along the edges to be aligned along the vertical direction.

The parametric study was performed to study the relationship between the model dimensions and the amplitude and natural frequency of the skin and to compare the FEA results with the analytical results derived earlier for this mode of actuation. The parametric study revealed that the amplitude values deviated more from the theoretical values with either decreasing *Length (L)* or with decreasing *Thickness (h)* of the skin. While cases of decreasing *Length* represent instances of greater violation of the long thin plate assumption on which the analytical estimate rests, decreasing *Thickness* represents cases in which the effect of the legs (which are not modeled in the analytical formulation) becomes more significant. So this trend is expected (

Table **1**). (Note: L = Wavelength of the traveling wave = twice the length of the Unit Cell = $2*l$)

Table 1. Comparison of analytical and FEA results for the deflection amplitude.

Thickness h in mm	Length L in mm	Deflection Amplitude in μm (from FEA)	Analytical Results (μm)	% Difference
1	25	4.82	5.16	7.1
0.75	25	10.66	12.23	14.8
0.5	25	32.42	41.29	25.4
1	35	9.58	10.12	5.6
0.75	35	21.46	23.98	11.8

The results of the parametric study using FEA are:

$$\text{Deflection Amplitude } \propto \frac{L^{2.04}}{h^{2.77}} \text{ from Finite Element Analysis } \left(\propto \frac{L^2}{h^3} \text{ from Theoretical calculations} \right)$$

Table 2. Comparison of analytical and FEA results for the Natural frequencies.

Thickness h in mm	Length L in mm	Natural Frequency in Hz (from FEA)	Analytical Results (Hz)	% Difference
1	25	10816.2	16043.1	48.3
0.75	25	7663.9	12031.7	57.0
0.5	25	4668.2	8021.5	73.2
1	35	6209.5	8185.3	31.8
0.75	35	4416.8	6138.9	39.0

A similar trend of greater deviation from the theoretical values with both decreasing *Length* and decreasing *Thickness* was observed in the values of the natural frequencies too. The deviations in this case were significantly larger, even though the analytical and FEA results were in the same order of magnitude (Table 3). The results of this parametric study were:

$$\text{Natural Frequency } \propto \frac{h^{1.22}}{L^{1.64}} \text{ from Finite Element Analysis} \left(\propto \frac{h}{L^2} \text{ from Theoretical calculations} \right)$$

The greater discrepancy between the analytical and the FEA results for the values of the natural frequency could be explained as the effect of the legs of the structure. The legs contribute to a reduction in the values of the natural frequencies by providing greater inertia to the structure without significantly increasing the stiffness to the structure. This claim is easily verified by performing FEA on 2 configurations of the skin that are identical in all respects except for the size of the legs. The skin dimensions used for this purpose were ***L*=25mm** and ***h*=1mm** with the material being Aluminum of E=70Gpa, ν=0.345 & ρ=2600 kg/m^3. The two sizes of the legs used were ***b*=1 mm** and ***b*=3 mm** long. The results were then compared to the values obtained from the analytical expressions, which essentially are cases of the skin with no legs attached. The results are tabulated below. It is clear that there is a reduction in the value of the first natural frequency with increase in the size of the legs. This confirms our argument that the inertia factor introduced by the legs is responsible for the disagreement in the two approaches.

Table 3. Effect of height of legs on Natural frequencies.

Cases	Natural Frequency in Hz
Theoretical (b=0)	16043.0
b = 1mm	13982.5
b = 3mm	10816.2

Shown below in Figure 8 is a typical contour plot of the axial stress distribution depicted on the plot of the deformed Unit Cell (deformations magnified by 50 times). It is clear from the nature of the distribution that it essentially

resembles the stress distribution in a beam subjected to a bending moment. Moreover the point of application of the force in the center leg hardly suffers any bending. This assumption, which was implicit in the analytical calculations, therefore stands verified. The first eigenmode of the Unit Cell is plotted in Figure 9 and shows that this mode shape is identical to the deflection pattern sought.

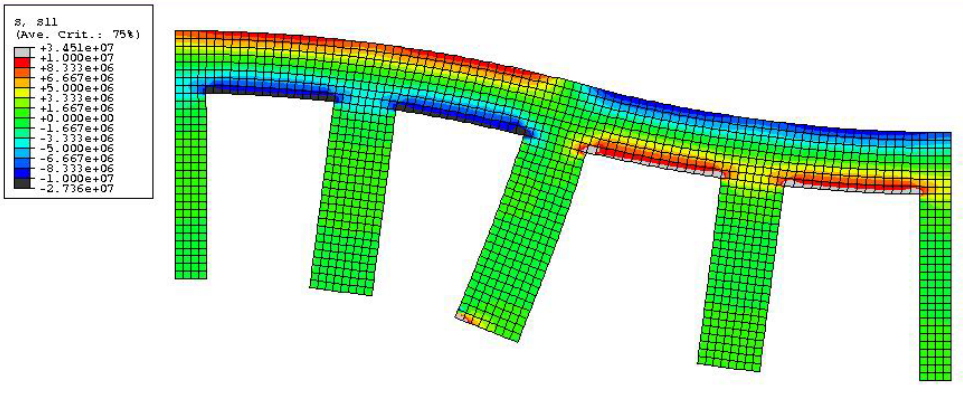

Figure 8. Contour plot of the stress distribution (along the direction of the wave).

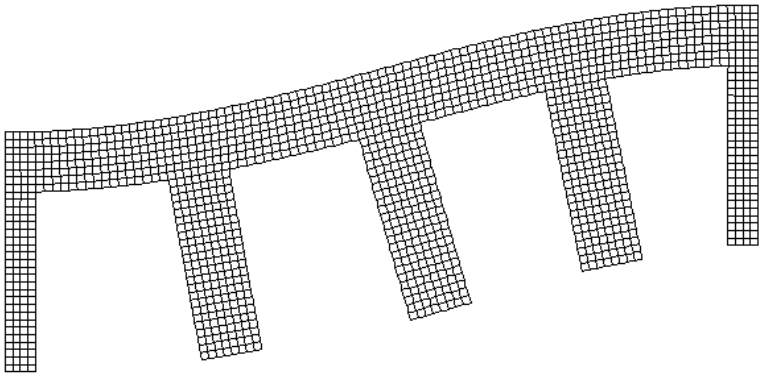

Figure 9. First eigenmode shape of the Unit Cell.

The Unit Cell hypothesis was verified by performing FEA of a model that was twice the length of the Unit Cell. The boundary conditions for this analysis were cyclic symmetry conditions at the ends since the model was one entire wavelength long. The results obtained thus exactly matched the earlier results confirming the validity of the Unit Cell hypothesis (Figure 10).

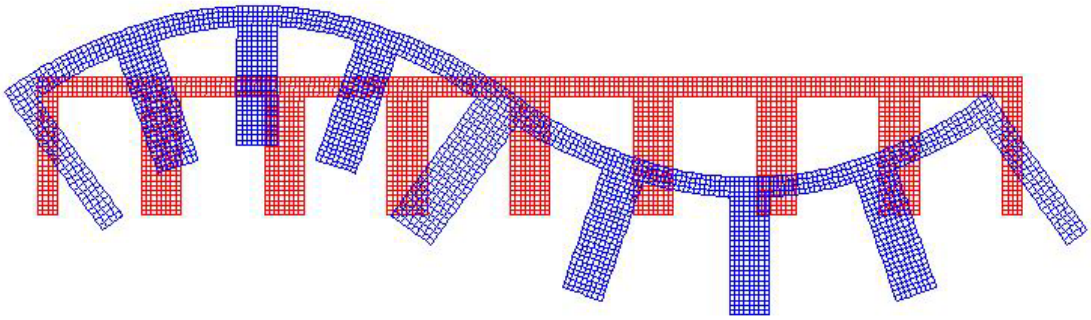

Figure 10. Deformed and Undeformed plots of twice the Unit Cell.

A few sample cases were analyzed using FEA for the Piezoceramic stack actuator based design to verify that the FEA results exactly matched the theoretical results. Since the assumptions made in the theoretical model are almost

the same as in the FEA this is expected. A minute deviation in the results is on account of the fact that the theoretical value is based on formulations derived from beam bending whereas the FEA results are obtained by solving a plane strain problem.

6. FEASIBILITY OF ACTIVE MATERIAL BASED ACTUATION

Based on the earlier studies it was decided to consider for the purpose of the feasibility study a skin of dimensions L=25mm, b=3mm, h=0.5mm, that is made of Aluminum of E=70Gpa and ν=0.345.

6.1 SMA actuation based design

A SMA wire (actuator) was incorporated into the Finite Element analysis using the subroutine developed by this research group to implement the behavior of SMAs into the finite element solver, ABAQUS. The subroutine numerically implements the unified thermomechanical constitutive model developed by Lagoudas et. al.[19] which was further refined by Bo and Lagoudas[7-10].

The analysis showed that a temperature change of 3^{o}C was sufficient in generating a deflection of amplitude = 32.58 μm. This corresponded to a reduction of the martensitic volume fraction from the initial value of 1 to 0.8739. However it should be noted that this result is for a skin of width = d = 1mm. It would be difficult to place one SMA wire for every mm so as to obtain the necessary deflections across the depth of the skin. One wire which actuated a section of skin of width = d = 5mm would be a more practical situation. Going by the analytical calculations it would be reasonable to expect that the force required when d = 5mm would be 5 times greater than that required for d = 1mm.

It was found that a temperature change of 5^{o}C was capable of producing a deflection of 31.2μm when the width of the skin was taken as 5mm. This also corresponded to a reduction in martensitic volume fraction to a value of 0.8677. and a strain of just 0.6%. This apparent lack of proportionality between the width of the skin and the temperature change is on account of the non-linear response of the SMA wire to temperature change.

It is quite possible to heat and cool the SMA wire back and forth by a temperature of 5^{o}C at relatively high frequencies. The efficiency of this cooling system can also be improved by using the cold air from the environment (in the case of aircraft). Even low flying UAVs such as the Predator operate at altitudes in the range of 10,000 feet. Taking the rate of drop in temperature with altitude as 6.5^{o}C/km, the temperature of the atmosphere at such altitudes would be close to the freezing point of water. This cold air can be used as part of a heat exchange mechanism to cool down the SMA wires quite rapidly. The rate of cooling can be improved further if the operating temperatures of the SMA wires are kept high, since the rate of cooling would be proportional to the temperature differential between the wire and air. By suitably adjusting the proportions of Ni and Ti in the SMA wire, it is possible to change the austenitic and martensitic start and finish temperatures to considerably high values. SMA based actuation therefore seems to possess considerable promise in this drag reduction technique.

Finally the life of the SMA at these low strains (0.6%) will be practically unlimited. Research has shown that at strain levels corresponding to partial phase transformation, several hundred thousands of actuation cycles can be performed before any SMA behavior deterioration can be observed. At levels of about 0.6% strain, even after millions of cycles, the SMA actuators are expected to be intact.

6.2 C-Block actuator based design

The force required for these parameters is F = 1N and deflection of the point of application of the force is 35.28 μm (in the legs). Going by the existing literature on C-Block actuators it is clear that these forces and displacements are well within the reach of C-Block actuators. However matching the geometric constraints of the active skin with the actuator might poses some challenges.

6.3 Piezoceramic stack actuator based design

The maximum force required for these parameters is F = 0.36N and corresponding deflection of the point of application = 30 μm. Commercially available stack actuators are well capable of delivering these requirements. However one significant disadvantage is that the lengths of these actuators need to be in the order of 40 mm to deliver the required displacements. This can create complications in embedding these systems in the airframe. Motion amplification mechanisms could resolve this problem but will introduce additional moving parts and design complications.

7. EXPERIMENTAL SETUP FOR VALIDATING THE DRAG REDUCTION TECHNIQUE

Each of the active skin designs discussed earlier, have issues that need to be addressed before a prototype can be built for testing purposes. In the case of piezoelectric C-block or piezoceramic stack actuators, meeting the geometric constraints is an immediate challenge. In the SMA based actuation mechanism, effective cooling systems need to be developed to achieve high actuation frequencies. In this section a mechanically actuated skin is introduced that was designed and fabricated for water-tunnel testing, to experimentally validate the drag reduction technique. This mechanically actuated skin is based on a cam actuation mechanism, which is significantly simpler and hence can be immediately built to test and validate the drag reduction theories.

The design utilizes a relatively simple mechanical version of a traveling sine wave using synchronized parallel plates driven via cam action. The design presented here uses three plates at 120-degree phase intervals. The individual plates are as thin as feasible, in order to minimize the wavelength of a given configuration. Plate thickness of 1/16" has been achieved so far.

This design divides a sine wave into 120-degree phase intervals by utilizing a three-stage cam as shown in Figure 11. Every fourth plate then has identical motion, and can be connected to one of three supports for synchronization. Cams then drive the supports at either end, producing the traveling wave. The three driving cams are then synchronized with shafts and timing belts. The shafts are supported by bearings on both sides of the cams, and a variable speed DC motor can drive either shaft. The bearings and motor are mounted on a bottom plate, which is not shown. The mechanically actuated skin has been designed and fabricated using the Rapid Prototyping facility available at the Department of Aerospace Engineering at Texas A&M University.

A 4"x4" section of the complete skin was developed and is shown in Figure 12. The mechanically actuated skin has been calibrated for testing and the vibrations caused due to cam action have been isolated. Actuation frequencies of 50 Hz have been achieved and the results of these experiments would be presented in future communications. Upon validation of this drag reduction technique using the mechanically actuated skin, any of the three active skin designs can be implemented on aerial vehicles.

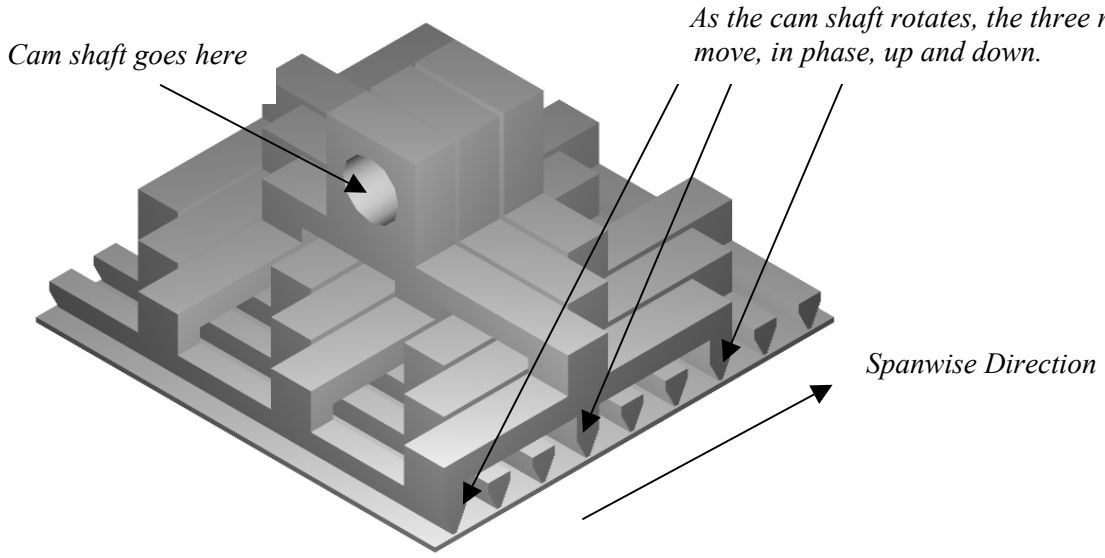

Figure 11. Solid modeling drawing for the active skin, illustrating its principles of operation.

8. CONCLUSIONS

A deformable active skin actuated by active materials has been proposed for a flow control technique that holds promise for large reduction in turbulent skin friction drag. Theoretical analyses of two design principles have been performed and were compared with FEA to come up with a parameterization of the deflection amplitude and the natural

frequency in terms of the model dimensions. The work efficiencies of the force based actuation scheme was found to be higher than those of the moment based actuation scheme from a structural point of view. Three different possible skin designs (that implement either of the two design principles) utilize SMA, piezoelectric C-block and piezoceramic stacks for actuation, respectively. It can be generally summarized that for applications in which the required actuation frequencies are low (order of 50 Hz for slow UAV applications), the SMA based actuation technique holds the greatest promise, whereas for applications involving high actuation frequencies (several hundred Hz, for airliners and military aircraft applications), the piezoelectric actuator based systems would be more appropriate. A mechanically actuated skin based on cam action has been designed and manufactured to test the validity the drag reduction technique prior to actual development of the active skin.

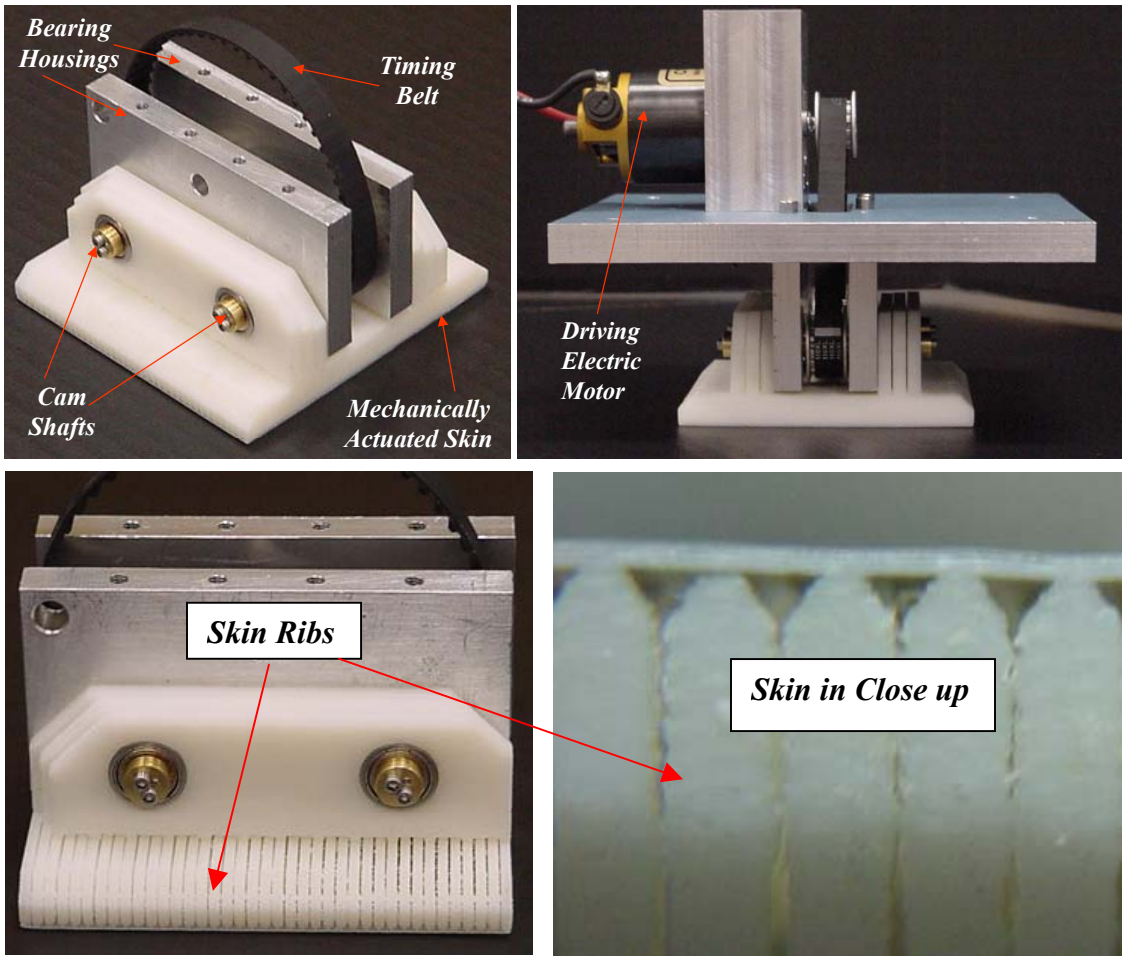

Figure 12. Pictures of the active skin showing the different components.

ACKNOWLEDGEMENTS

The authors would like to acknowledge the financial support of NASA Langley, Virginia, Grant No. F49620-01-1-0196. The authors would also like to thank Mike Walsh, the technical monitor for the project.

REFERENCES

1. D.W. Bechert, M. Bartenwerfer, G. Hoppe, and W.-E. Reif, “Drag reduction mechanisms derived from shark skin,” Paper 86-1.8.3.15th Congress, *International Council of Aeronautical Sciences*, London, 1986.

2. D.W. Bechert and M. Bartenwerfer, “The viscous flow on surfaces with longitudinal ribs,” *Journal of Fluid Mechanics*, Vol. 206, pp.105-129, 1989.
3. Y. Du and G.E. Karniadakis, “Suppressing Wall Turbulence by Means of a Transverse Traveling Wave,” *Science Reprint*, Vol. 288, pp. 1230-1234, 2000.
4. B.G. Kaufmann and I. Mayo, “The metal with a memory.” *Invention and Technology*, Fall 18-23, 1993.
5. W.J. Buehler and R.C. Wiley, *Nickel-base Alloys US Patent 3,174,851*, 1965
6. C.M. Jackson, H.J. Wagner and R.J. Wasilewski, “55-Nitinol – The Alloy with a Memory: its Physical Metallurgy, Properties, and Applications,” *NASA-SP 5110*, 1972.
7. Z. Bo and D. C. Lagoudas, “Thermomechanical modeling of polycrystalline SMAs under cyclic loading, part I: theoretical derivations,” *International Journal of Engineering Science*, Vol. 37, pp. 1089-1140, 1999a.
8. D.C. Lagoudas and Z. Bo, “Thermomechanical modeling of polycrystalline SMAs under cyclic loading, part II material characterization and experimental results for a stable transformation cycle,” *International Journal of Engineering Science*, Vol. 37, pp. 1141-1174, 1999.
9. Z. Bo and D.C. Lagoudas, “Thermomechanical modeling of polycrystalline SMAs under cyclic loading, part III: evolution of plastic strains and two-way memory effect,” *International Journal of Engineering Science*, Vol. 37, pp. 1175-1204, 1999b.
10. Z. Bo and D.C Lagoudas, “Thermomechanical modeling of polycrystalline SMAs under cyclic loading, part IV: modeling of minor hysteresis loops,” *International Journal of Engineering Science*, Vol. 37, pp. 1205-1249, 1999c.
11. Z. Bo, D.C. Lagoudas and D.A. Miller, “Material Characterization of SMA Actuators Under Non-Proportional Thermomechanical Loading,” *Journal of Engineering Materials and Technology*, Vol.121, No. 1, pp. 75-85, 1999.
12. Y. Sato and K. Tanaka, “Estimation of energy dissipation in alloys due to stress-induced martensitic transformation,” *Res Mechanica* Vol. 23, pp. 381-393, 1988.
13. C. Liang and C.A. Rogers, “One-dimensional thermomechanical constitutive relations for Shape Memory Materials,” *Proceedings 31st AIAA/ASME/ASCE/AHS/ASC Structures, Structural Dynamics and Materials Conference* (Long Beach, CA), AIAA-90-1027, 1990.
14. C. Liang and C.A. Rogers, “Multi-dimensional constitutive relations of shape memory alloys,” *Proceedings, AIAA 32nd Structures, Structural Dynamics and Materials Conference* (Baltimore, MD), 1991.
15. E. Patoor, A. Eberhardt and M. Berveiller, “Micromechanical modeling of superelasticity in Shape Memory Alloys,” *Journal de Physique* IV, Vol. 6 C1, pp. 277-292, 1996.
16. J.G. Boyd and D.C. Lagoudas, “A thermodynamic constitutive model for the Shape Memory Materials. Part I. The monolithic Shape Memory Alloys,” *International Journal of Plasticity*, Vol. 12 No. 6 pp. 229-242, 1996.
17. S. Leclercq and C. Lexcellent, “A general macroscopic description of the thermomechanical behavior of Shape Memory Alloys,” *Journal of Mechanics of the Physics of Solids*, Vol.44 No. 6 pp. 953-980, 1996.
18. L.C. Brinson, “One-dimensional constitutive behavior of Shape Memory Alloys: Thermomechanical derivation with non-constant material functions and redefined martensite internal variable,” *Journal of Intelligent Material Systems and Structures*, Vol. 4 pp. 229-242, 1993.
19. D.C. Lagoudas, Z. Bo and M.A. Qidwai, “A unified thermodynamic constitutive model for SMA and Finite Element Analysis of active metal matrix composites,” *Mechanics of Composite Materials and Structures*, Vol. 3, pp. 153-179, 1996.
20. V. Birman, “Review of Mechanics of Shape Memory Alloy Structures,” *Applied Mechanics Reviews*, Vol. 50, No.11, pp. 629-645, 1997.
21. A. Chattopadhyay, C. Seeley and L. Mitchell, “Design of a Smart Flap Using Polymeric C-Block Actuators and a Hybrid Optimization Technique,” *Journal of Smart Materials and Structures*, Vol. 6, pp. 134 – 144, 1997.
22. A. Chattopadhyay, H. Gu and D. Dragomir-Daescu, “Dynamics Of Delaminated Composite Plates With Piezoelectric Actuators,”, *AIAA Journal*, Vol. 37, No. 2, pp. 248 – 254, 1999.
23. A.J. Moskalik and D. Brei, “Force-deflection behavior of piezoelectric C-block actuator arrays,” *Smart Materials and Structures*, Vol. 8(5) pp. 531-543, 1999.
24. C. Shakeri, M.N. Noori and Z. Hou, "Smart Materials and Structures: A Review," *Proceedings of the Fourth Materials Engineering Conference* (Washington, D.C.), Vol. 2, pp. 863-876, November 1996.
25. J.N. Reddy, *Theory and Analysis of Elastic Plates*, Library Binding, Taylor & Francis, 1999
26. S. Timoshenko, *Theory of Plates and Shells*, McGraw-Hill, 1940.
27. E.P. Popov, *Engineering Mechanics of Solids*, Prentice-Hall, 1996.
28. S. Timoshenko, *Vibration Problems in Engineering*, D.Van Nostrand Company Inc, 1940.